

International Journal of Quantum Information
 © World Scientific Publishing Company

TOWARD THIRD ORDER GHOST IMAGING WITH THERMAL LIGHT

G. BRIDA, I. P. DEGIOVANNI, G. A. FORNARO, M. GENOVESE, A. MEDA

*Istituto Nazionale di Ricerca Metrologica (INRIM), Strada delle Cacce 91,
 Torino 10135, Italy
 a.meda@inrim.it*

Received Day Month Year

Revised Day Month Year

Recently it has been suggested that an enhancement in the visibility of ghost images obtained with thermal light can be achieved exploiting higher order correlations¹. This paper reports on the status of an higher order ghost imaging experiment carried on at INRIM labs exploiting a pseudo-thermal source and a CCD camera.

Keywords: quantum imaging

1. Introduction

Quantum Imaging is a new quantum technology addressed to exploit properties of quantum optical states for overcoming limits of classical optics².

Various protocols have been recently proposed^{3,4,5,6,7,8} and realized^{9,10,11,12,13,14} ranging from super-resolution to sub-shot noise imaging.

One of the oldest ideas, that can find very interesting applications¹⁵, is the so called Ghost Imaging. In summary, the idea at the basis of this protocol is that whether one disposes of two noise-correlated light beams, one crossing an object to be imaged and then detected by a bucket detector without any spatial resolution, the other addressed to a spatial resolving detector (as a CCD camera), then the image of the object can be reconstructed by considering correlations between the two measurements.

This protocol was firstly predicted¹⁶ and then demonstrated with twin beams¹⁷ and later with thermal light^{18,19,20,21} (with only a smaller visibility).

Recently, it was shown that the use of higher order correlation functions can improve the visibility of ghost imaging¹.

A first experiment in this sense was realized in²². This interesting result, nevertheless, was valid only in the approximation of very high light flux where $G^{(3)}$ was reconstructed by a $G^{(2)}$ measurement and was realized with a "fake" mask (i.e. by artificially blackening some pixels of the camera via software). Very recently a second experiment appeared where a real object (a double slit) was imaged through a scan that allowed to reconstruct $G^{(3)}$ ²³.

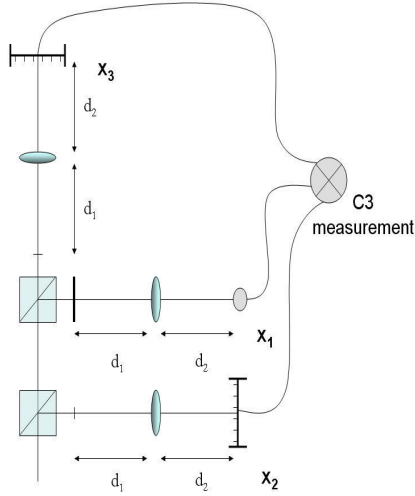


Fig. 1. Third order imaging scheme. There are two reference arms and a test arm. Distances d_1 and d_2 have to satisfy the imaging condition. The detectors on the reference arms are spatially resolving while in the test arm a bucket detector is present.

Here we present our preliminary results toward third order correlation Ghost Imaging reconstruction of a real object observed through a CCD camera and compare the achieved results with second order ghost imaging ones.

2. Theory

The imaging scheme (Fig. 1) counts three arms, two reference arms and a test arm. The unknown object is inserted in the latter. Each distinct imaging system is characterized by its impulse response function $h_i(x'_i, x_i)$, where $i = 1, 2, 3$, x'_i are the starting transverse coordinates and x_i are the coordinates at the detection plane. Hence, considering a field $E_i(x'_i)$, its value at the detection plane is given by:

$$E_i(x_i) = \int dx'_i h_i(x'_i, x_i) E_i(x'_i) \quad (1)$$

In our scheme the subscript $i = 1$ refers to the test arm.

The detectors in the reference arms are spatially resolving detectors and record the intensity distribution $I_2(x_2)$ and $I_3(x_3)$ in the pixel x_2 and x_3 respectively.

Information about the object is obtained by measuring the (normalized) second order correlation coefficient $c2$ in the case of second order ghost imaging and the (normalized) third order coefficient $c3$ in the case of third order ghost imaging, defined as:

$$c2(x_1, x_j) = \frac{\langle I_1(x_1)I_j(x_j) \rangle - \langle I_1(x_1) \rangle \langle I_j(x_j) \rangle}{\sqrt{\mu_2(x_1)}\sqrt{\mu_2(x_j)}} \quad (2)$$

with $j = 2, 3$ and:

$$c3(x_1, x_2, x_3) = \frac{\langle (I_1(x_1) - \langle I_1(x_1) \rangle)(I_2(x_2) - \langle I_2(x_2) \rangle)(I_3(x_3) - \langle I_3(x_3) \rangle) \rangle}{\sqrt[3]{\mu_3(x_1)}\sqrt[3]{\mu_3(x_2)}\sqrt[3]{\mu_3(x_3)}} \quad (3)$$

where $\langle I_i(x_i) \rangle = \langle E_i^*(x_i)E_i(x_i) \rangle$ is the mean intensity of the i -th beam. In formula (2) we define:

$$\mu_2(x_i) = \langle (I_i(x_i) - \langle I_i(x_i) \rangle)^2 \rangle \quad (4)$$

as the second central moment, while in (3)

$$\mu_3(x_i) = \langle (I_i(x_i) - \langle I_i(x_i) \rangle)^3 \rangle \quad (5)$$

is the third central moment. Symbols $\langle .. \rangle$ refers to temporal averages. As a matter of fact it is the correlation between the beams which is responsible of the image formation in the ghost imaging process^{2,24}, for this reason we considered the (normalized) correlation coefficient $c2$ and $c3$ instead of the $G^{(2)}$ and $G^{(3)}$ functions. In fact, this is helpful as it removes unwanted effects related to the unbalancing of the intensity or of the fluctuations between the beams which may somehow hide the correlations of interest.

3. Experimental set-up

In our experiment (Fig. (2)), the imaging system consists of three classical correlated thermal light beams. The thermal field is obtained by passing a coherent source through a random media. The source is a passively Q-switched microchip laser with a pulse duration of about 1 ns and a maximum average power of 1 W; this source together with a frequency doubler (the second harmonic generator in the figure) produces a 532 nm beam. The prism deflects the first harmonic (1064 nm) beam to a beam stopper. The 532 nm source is scattered by a rotating ground glass disk (the random media) in order to obtain the pseudo-thermal field. The beam is then split in three beams by means of two beam splitters (a polarizing beam splitter BS1 and a non-polarizing beam splitter BS2) and a 45° mirror and sent to a EMCCD camera. The presence of the half waveplate WP on the path of the beam before the rotating disk, together with the polarizing beam splitter, allows to balance the intensities on the three arms.

The dimension of the coherence areas of the multimode thermal beams are set by the lens L1 of focal length $f = 750$ mm. The lens is put in a $f - f$ configuration

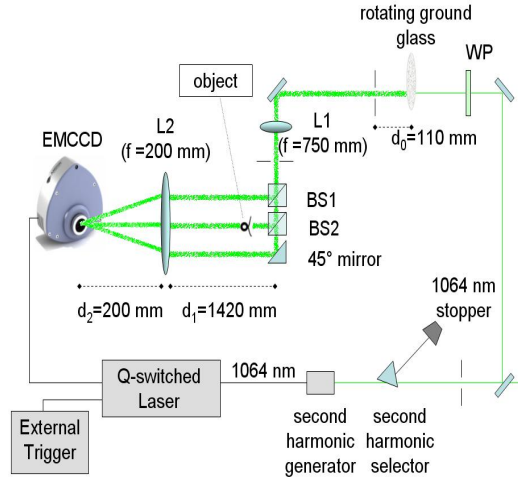


Fig. 2. Experimental set-up.

respect to the pinhole and to the object in order to observe the far field speckle pattern at the plane with the object. In this way, a single transverse wavevector q is associated to a single point $x = (\lambda f / 2\pi)q$. The pinhole is at distance $d_0 = 110$ mm from the rotating ground glass. As a matter of fact, the dimension of the coherence areas is also proportional, for a given wavelength, to the distance between the ground glass and the pinhole and inversely to the dimension of the pinhole. A second pinhole after L1 determines the dimension of the source.

The lens L2 before the camera is used to image the beams on the CCD. A magnification occurs in order to image the whole area of the three beams on the 658×498 pixels sensitive area of the CCD, that is $6,58 \text{ mm} \times 4,98 \text{ mm}$ since the pixel area is $10 \text{ } \mu\text{m} \times 10 \text{ } \mu\text{m}$. Distances $d_1 = 1420$ mm and $d_2 = 200$ mm are chosen in order to obtain a proper demagnification.

The camera is triggered with the pulses of the laser. The repetition rate of the laser is externally set to 500 Hz, while the exposure time of the camera is of 2 ms. Since the pulse duration is no longer than 1 ns, each frame taken with the CCD contains only one pulse of the laser. The ratio between the repetition rate of the camera and the frequency of rotation of the disk avoids a periodic speckle

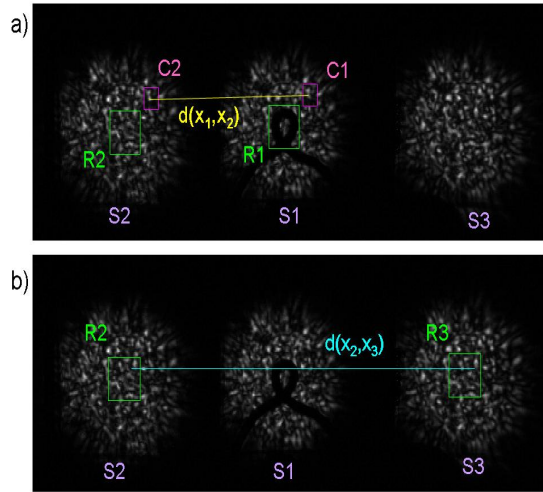


Fig. 3. The image of the three thermal beams from a single shot of the laser a) Correlated regions in arm 1 and 2. b) Correlated regions in arm 2 and 3.

pattern detection. Moreover, the disk has to rotate slowly enough to be considered stationary with respect to the duration of the pulse of the laser.

The object is an iron curled wire with a diameter of 1.5 mm.

4. Toward third-order ghost imaging: experimental results

Fig. (3) reports the image obtained from a single shot of the laser. We can appreciate the speckle structure and the correlations in its intensity on the three thermal beams. The object is in the central arm, named S_1 ; S_2 and S_3 denotes the reference arms. In order to retrieve information about the correlations, the first step is to determine with high precision the regions R_2 and R_3 correlated to the one with the object, R_1 (Fig. (3) a)). Due to the presence of the object, we first determine the distance $d_{1,2}$ between R_1 and R_2 using a region C_1 without the object and finding the correlated one, C_2 in the arm 2. Starting from a region $C_{2,0}$ of S_2 we displace the region in horizontal and vertical directions, pixel by pixel, in order to find the maximum of the normalized second order correlation coefficient (2) for a frame k :

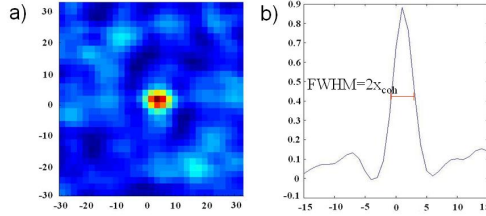


Fig. 4. a) The correlation coefficient as a function of the displacement vector D b) The peak of correlation. Its FWHM represents the diameter of the speckle

$$c2^k = \frac{\langle I_1^{(k)}(x_1) I_2^{(k)}(x_{2,0} + D) \rangle - \langle I_1^{(k)}(x_1) \rangle \langle I_2^{(k)}(x_{2,0} + D) \rangle}{\sqrt{\mu_2(x_1)} \sqrt{\mu_2(x_{2,0} + D)}} \quad (6)$$

where $I_1^{(k)}(x_1)$ and $I_2^{(k)}(x_{2,0})$ are the intensities of the frame k for the region C_1 and $C_{2,0}$ respectively. D is the displacement vector in pixel. In Eq. (7) the symbol $\langle .. \rangle$ refers to spatial averages over the pixels of the selected regions. The distance between the correlated regions is computed as: $d_{1,2} = |x_1 - x_2|$, with $x_2 = x_{2,0} + D_{max}$, where D_{max} correspond to the displacement to be applied in order to reach the maximum of the correlation. Finally we determine the region R_3 correlated to R_2 using the same procedure (Fig. 3 b)).

The correlation coefficient as a function of the displacement vector D is depicted in Fig. (4) a); the part b) of the figure reports the section of the peak of correlation in the horizontal direction. The reported correlation between the regions is quite high (~ 0.88), denoting a low level of losses in the optical path and low noise. The FWHM of the peak is a good estimation of the size of a speckle; in our experiment we generate speckles of radius $x_{coh} \approx 3$ pixels = $30 \mu\text{m}$.

To perform ghost imaging, we use a bucket detector on arm 1. For each frame k taken with the camera, the measured quantity in arm 1 is then the integral over x_1 : $I_1^{(k)} = \int dx_1 I_1^{(k)}(x_1)$. In practice, it corresponds to the sum over the pixels of the region R_1 with the object. The intensity distributions of the correlated regions

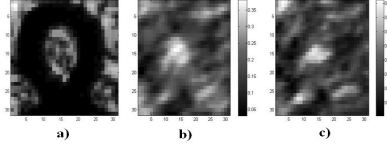


Fig. 5. a) The image of the real object b) The second order ghost image c) The third order ghost image

on the other arms are registered as an array of intensity values $I_j^{(k)}(x_j)$.

We reconstruct normalized second and third order correlation functions $c2$ and $c3$ as the ghost images of our real object. For $c2$ we used arm 2 and arm 3 alternatively as reference. Fig. (5) shows our preliminary results. Part a) of the figure reports the single frame image of the object in the region R_1 , while part b) shows one of the two reconstructed images by means of $c2$. Finally, the c) part is the third order ghost imaging of the object. The correlation coefficients are computed averaging over $N_f = 400$ frames. The reconstructed images are evident even if the resolution is quite low. This can be understood once you consider that the speckles have a diameter of 6 speckles, i.e. a dimension comparable to the one of the object (i.e. tens of speckles according to Fig. (5) a))

As a figure of merit to estimate the improvement of third order ghost imaging respect to second order one we chose the visibility of the reconstructed images, here defined as:

$$V_j = \frac{c_{jback} - c_{jobj}}{c_{jback} + c_{jobj}} \quad (7)$$

with $j = 2, 3$, where c_{jback} is the value of the correlation coefficient averaged over a region without the object and c_{jobj} is computed averaging over a region with the reconstructed object.

We obtain $V_2 = 0.2301 \pm 0.0008$ (the result is independent by the choice of arm 2 or 3 as reference) and $V_3 = 0.269 \pm 0.006$. It is clear that there is an improvement in the value of the visibility of the reconstructed image by means of third order correlations. It was theoretically predicted by Bai et al.¹ that the existence of ad-

ditional correlation parts, namely correlations between the two reference detectors and between the three detectors, leads to an improvement of the visibility. Our experimentally measured increment in the value of V_3 with respect to V_2 can be compared to their theoretical predictions. Moreover, the gap remains stable even if we use different set of images. We also observe that the number of frames used to reconstruct the image is sufficient to reach the maximum gap. An increment of the number of frames do not lead to an improvement of the ghost imaging performances. In any case, we want to stress that the reported data are a preliminary experimental demonstration of the improvement in the visibility and that a more complete analysis is postponed to a subsequent paper.

5. Conclusions

In this paper we have presented a realization of third order ghost imaging of a real object exploiting a CCD camera. We also show an improvement in the visibility of third order ghost imaging respect to second order one. Having overcome some limits of previous experiments, it represents a relevant step toward real applications of ghost imaging¹⁵.

Acknowledgments

We thank M. Chekhova for useful discussions.

References

1. Y. Bai and S. Han, Phys. Rev. A **76** (2007) 043828.
2. L. Lugiato et al., J.Opt.B **4** (2002) S176-S183;
3. A. Boto et al, Phys. Rev. Lett. **85**(2000) 2733-2736;
4. A. Gatti et al., Phys. Rev. Lett. **83** (1999) 1763-1766;
5. S. Tan et al., Phys. Rev. Lett. **101** (2008) 253601;
6. V.Giovannetti et al., Phys. Rev. A **79** (2009) 013827;
7. E. Brambilla et al., Phys. Rev. A **77** (2008) 053807;
8. I.Santos et al., Phys. Rev. A **67** (2003) 033812;
9. M. Genovese, Research on hidden variable theories: a review of recent progresses, ed. J. Eichler (ENSEVIER, Netherlands, 2005);
10. G. Brida et al., arXiv1005.3665;
11. G. Brida et al., Nature Photonics **4** (2010) 227-230;
12. M. D'Angelo et al., Phys. Rev. Lett. **87** (2001) 013602;
13. Mosset et al., Phys. Rev. Lett. **94** (2005) 223603;
14. I.Santos et al., Phys. Rev. A **77** (2008) 043832;
15. R. Meyers et al., Phys. Rev. A **77** (2008) 041801.
16. A. Belinskii D.Klyshko, Sov. P.JETP **78** (1994) 259.
17. T.Pittman et al., Phys. Rev. A **52** (1995) R3429-R3432;
18. R. Bennik et al., Phys. Rev. Lett. **85** (2002) 113601;
19. F. Ferri et al., Phys. Rev. Lett. **94** (2005) 183602;
20. A. Valencia et al., Phys. Rev. Lett. Vol. **94** (2005) 063601;
21. Y. Zhou et al., Phys. Rev. A **72** (2005) 043805;

22. Agafonov et al., arXiv:0911.3718v2.
23. Y. Zhou et al., Phys. Rev. A **81** (2010) 043831.
24. I. P. Degiovanni et al., Phys. Rev. A **76**, 062309 (2007)